CHEMISTRY OF MATERIALS
Article

Chem. Mater. **2010,** *22,* 3399–3406 3399
DOI:10.1021/cm100058q

Investigation of Cu_2ZnSnS_4 Formation from Metal Salts and Thioacetamide

Achim Fischereder,[†,‡] Thomas Rath,[†,‡] Wernfried Haas,[‡,§] Heinz Amenitsch,[⊥] Jörg Albering,[†] Dorith Meischler,[†] Sonja Larissegger,[†,‡] Michael Edler,[†,‡] Robert Saf,[†] Ferdinand Hofer,[§] and Gregor Trimmel*[,†,‡]

[†]*Institute for Chemistry and Technology of Materials, Graz University of Technology, Stremayrgasse 16, 8010 Graz, Austria,* [‡]*Christian Doppler Pilotlaboratory for Nanocomposite Solar Cells, Graz University of Technology and NanoTecCenter Weiz Forschungsgesellschaft mbH, Austria,* [§]*Institute for Electron Microscopy and Fine Structure Research, Graz University of Technology, Steyrergasse 17, 8010 Graz, Austria, and* [⊥]*Institute of Biophysics and Nanosystems Research, Austrian Academy of Sciences, Schmiedlstrasse 6, 8042 Graz, Austria*

Received January 7, 2010. Revised Manuscript Received April 28, 2010

Copper zinc tin sulfide (Cu_2ZnSnS_4, CZTS) is a very promising alternative to semiconductors based on Ga or In as solar absorber material. CZTS consists of abundant and cheap elements and in addition it displays very beneficial properties like a high optical absorption coefficient and an ideal band gap for photovoltaic applications. In this contribution, we present the preparation of thin films of copper zinc tin sulfide from metal salts (copper(I) iodide, zinc(II) acetate, and tin(II) chloride) and thioacetamide as sulfur source by a solution-based precursor method. The influence of synthesizing temperatures and concentration of thioacetamide in the precursor solution on the obtained CZTS materials was investigated. X-ray diffraction studies show that kesterite CZTS is formed. Depending on the temperature, nanocrystalline films with primary crystallite sizes from 8 nm (180 °C) up to approximately 150 nm (450 °C) were obtained. The early stages of the CZTS formation were monitored by time-resolved simultaneous grazing incident small- and wide-angle X-ray scattering (GISAXS, GIWAXS) analysis directly in thin layers revealing that the thermally induced reaction already starts at approximately 105 °C. The thin films exhibit high optical absorption ($> 1 \times 10^4$ cm^{-1}) and an optical band gap between 1.41 and 1.81 eV depending on the heat treatment. The obtained CZTS materials are of copper-poor and zinc-rich nature, which is ideal for the use in photovoltaic applications.

Introduction

Chalcopyrite-type semiconductors like $Cu(In,Ga)S_2$ or $Cu(In,Ga)Se_2$ have very beneficial properties for photovoltaic applications,[1,2] which led in turn to a strong scientific interest in thin film solar cells based on these materials. Obtained efficiencies are remarkably high, up to nearly 20%;[3] however, gallium and indium used for the preparation of the active layer are very rare and expensive elements. This could lead to a shortage in the supply of these elements and would inhibit a cost-effective large-scale production.[4] To overcome these limitations, alternative materials are heavily researched in order to substitute the expensive elements In and Ga. Among these materials, Cu_2ZnSnS_4 (CZTS) is one of the most promising materials as it consists of abundant and relatively cheap elements. This semiconductor combines the properties for an ideal absorber layer for photovoltaic applications, like a direct band gap of about 1.4−1.5 eV[5−7] and an optical absorption coefficient higher than 1×10^4 cm^{-1}.[8,9] Mainly two general approaches have been used in the recent years for the preparation of CZTS thin films: physical vapor methods and chemical deposition methods. Examples for physical vapor methods are thermal evaporation of the elements and binary chalcogenides,[10] sulfurization of electronbeam evaporated metallic layers,[11,12] as well as

*Corresponding author. E-mail: gregor.trimmel@tugraz.at. Tel: +43-316-8738458. Fax: +43-316-8738951.

(1) Kaelin, M.; Rudmann, D.; Tiwari, A. N. *Sol. Energy* **2004**, *77*, 749–756.
(2) Kois, J.; Ganchev, M.; Kaelin, M.; Bereznev, S.; Tzvetkova, E.; Volobujeva, O.; Stratieva, N.; Tiwari, A. N. *Thin Solid Films* **2008**, *516*, 5948–5952.
(3) Repins, I.; Contreras, M. A.; Egaas, B.; DeHart, C.; Scharf, J.; Perkins, C. L.; To, B.; Noufi, R. *Prog. Photovoltaics* **2008**, *16*, 235–239.
(4) Scragg, J. J.; Dale, P. J.; Peter, L. M.; Zoppi, G.; Forbes, I. *Phys. Status Solidi B* **2008**, *245*, 1772–1778.
(5) Todorov, T.; Kita, M.; Carda, J.; Escribano, P. *Thin Solid Films* **2009**, *517*, 2541–2544.
(6) Yeh, M. Y.; Lee, C. C.; Wuu, D. S. *J. Sol−Gel Sci. Technol.* **2009**, *52*, 65–68.
(7) Seol, J. S.; Lee, S. Y.; Lee, J. C.; Nam, H. D.; Kim, K. H. *Sol. Energy Mater. Sol. Cells* **2003**, *75*, 155–162.
(8) Ito, K.; Nakazawa, T. *Jpn. J. Appl. Phys.* **1988**, *27*, 2094–2097.
(9) Kishore Kumar, Y. B.; Suresh Babu, G.; Uday Bhaskar, P.; Sundara Raja, V. *Sol. Energy Mater. Sol. Cells* **2009**, *93*, 1230–1237.
(10) Friedlmeier, T. M.; Dittrich, H.; Schock, H. W. *Inst. Phys. Conf. Ser.* **1998**, *152*, 345–348.
(11) Araki, H.; Mikaduki, A.; Kubo, Y.; Sato, T.; Jimbo, K.; Maw, W. S.; Katagiri, H.; Yamazaki, M.; Oishi, K.; Takeuchi, A. *Thin Solid Films* **2008**, *517*, 1457–1460.
(12) Katagiri, H.; Sasaguchi, N.; Hando, S.; Hoshino, S.; Ohashi, J.; Yokota, T. *Sol. Energy Mater. Sol. Cells* **1997**, *49*, 407–414.

Published on Web 05/13/2010

Rf sputtered precursor layers,[13] Rf magnetron sputtering,[7] coevaporation,[14] and hybrid sputtering.[15] Chemical methods involve sulfurization of electrochemically deposited metal precursors,[4,16−18] photochemical deposition,[19] sol−gel sulfurization methods,[20,21] sol−gel spin-coated deposition,[6] and spray pyrolysis.[9,22−24] In addition, CZTS nanocrystals were prepared by solution-based synthesis[25,26] and were recently used for the fabrication of CZTS absorber films in photovoltaic devices.[27] Typically thiourea is used as the sulfur source for the deposition of CZTS and related sulfides in solution-based methods. However, the obtained CZTS films contain very often other sulfide phases or unidentified impurities,[6,9,22,24] In addition, thiourea tends to form organic byproducts that are even present when relatively high annealing temperatures of 380 °C are used.[28]

In this contribution, we present an alternative synthesis route for the preparation of CZTS layers prepared by a solution-based coating process using metal salts and pyridine. As sulfur source thioacetamide (TAA) was used, which should minimize organic impurities of the material, more volatile decomposition products are formed, which finally should lead to pure CZTS materials. In addition, this should allow reducing the synthesizing temperature, at which single-phase CZTS can be obtained. Within this work, we evaluate the influence of different synthesizing temperatures and amounts of TAA by using various analytical methods: X-ray diffraction (XRD), optical absorption spectroscopy, energy dispersive X-ray spectroscopy (EDX), scanning electron microscopy (SEM), and a surface profiler. To gain a better insight into the early stages of formation of CZTS films and to determine the temperature at which the CZTS formation starts, we performed an in situ time- and temperature-resolved synchrotron X-ray analysis.

Experimental Section

Chemicals. Copper(I) iodide (CuI, 99,999%), zinc(II) acetate ($ZnAc_2$, 99,99%), tin(II) chloride anhydrous ($SnCl_2$, ≥97%), thioacetamide (TAA, 99+%), and pyridine (reagent plus ≥99%) were purchased from Sigma Aldrich and used without further purification.

Indium tin oxide (ITO)-coated glass substrates with a surface resistivity of 15−25 ohm/cm^2 were purchased from Delta Technologies Ltd.

Sample Preparation. ITO-coated glass substrates were cleaned in an ultrasonic water bath followed by an ultrasonic isopropanol bath, each for 20 min. The CZTS precursor solution consisted of CuI (0.32 mol/L), $ZnAc_2$ (0.16 mol/L), $SnCl_2$ (0.16 mol/L), and TAA (3.2 mol/L or 2.2 mol/L) dissolved in pyridine. The solution was then spin-coated at a speed of 1500 rpm on the substrates, which were then baked for 15 min at different temperatures in the range of 180−450 °C (heating rate 21 °C/min) under vacuum to form the CZTS-layer. After the heat treatment, the samples were cooled to room temperature under a vacuum within 10 min.

For XRD analysis and TEM-EDX measurements, the CZTS-precursor solution was sprayed onto glass substrates at ambient conditions, followed by the same heat treatment of the substrates as described above. Finally, the micrometer-thick CZTS layer was scraped off the glass substrate to obtain the CZTS powder.

Characterization. The X-ray powder diffraction profiles were measured with a Siemens D-5005 powder diffractometer (θ/θ geometry, Cu Kα radiation, graphite monochromator, scintillation counter, step width 0.02°, constant counting times of 10 s/step, measured range of 20−60° in 2θ). The diffraction patterns were fitted by full-profile Rietveld refinements using the program system TOPAS 3. The calculations included least-squares refinements of the profile parameters (lattice constants, sample height, six parameters for Pseudo-Voigt approximations of the peak profiles and − in separate cycles − the crystallographic domain sizes) as well as structural data (positional and displacement parameters, occupancies). Transmittance and reflectance spectra of the thin films were measured with a Lambda900 spectrometer (Perkin-Elmer) including an external integrating sphere diffuse reflectance accessory (PELA-1000). The surface morphology was studied with a Veeco Dektak 150 surface profiler and a JEOL JSM-5410 scanning electron microscope equipped with a secondary electron detector. Energy dispersive X-ray (EDX) spectra were recorded in scanning transmission electron microscopy (STEM) mode using a Philips CM20/STEM operated at 200 kV with a LaB_6 cathode equipped with a Noran HPGe-detector. Simultaneous 2D grazing incident small-angle X-ray scattering (GISAXS) and 1D gracing incident wide-angle X-ray scattering (GIWAXS) measurements were performed at the Austrian SAXS Beamline 5.2 L of the electron storage ring ELETTRA (Italy).[29] The beamline has been adjusted to a q-resolution ($q = 4\pi/\lambda * \sin(2\theta/2)$) between 0.1 and 3.1 nm^{-1} (GISAXS) and to resolve the angular range (2θ) between 21.1° and 41.8° (GIWAXS) using an X-ray energy of 8 keV. The glass/ITO/precursor-substrates were placed in a custom-made sample cell with a grazing angle of about 0.18° and were heated from 40 °C up to 180 °C at a heating rate of approximately 8 °C/min in vacuum. During the temperature scan, data were recorded with 5 and 10 s resolution for GISAXS and GIWAXS, respectively.

(13) Jimbo, K.; Kimura, R.; Kamimura, T.; Yamada, S.; Maw, W. S.; Araki, H.; Oishi, K.; Katagiri, H. *Thin Solid Films* **2007**, *515*, 5997–5999.
(14) Tanaka, T.; Kawasaki, D.; Nishio, M.; Guo, Q.; Ogawa, H. *Phys. Status Solidi C* **2006**, *3*, 2844–2847.
(15) Tanaka, T.; Nagatomo, T.; Kawasaki, D.; Nishio, M.; Guo, Q.; Wakahara, A.; Yoshida, A.; Ogawa, H. *J. Phys. Chem. Solids* **2005**, *66*, 1978–1981.
(16) Kurihara, M.; Berg, D.; Fischer, J.; Siebentrit, S.; Dale, P. J. *Physica Status Solidi C* **2009**, *6*, 1241–1244.
(17) Ennaoui, A.; Lux-Steiner, M.; Weber, A.; Abou-Ras, D.; Koetschau, I.; Schock, H.-W.; Schurr, R.; Hoelzing, A.; Jost, S.; Hock, R.; Voss, T.; Schulze, J.; Kirbs, A. *Thin Solid Films* **2009**, *517*, 2511–2514.
(18) Araki, H.; Kubo, Y.; Mikaduki, A.; Jimbo, K.; Maw, W. S.; Katagiri, H.; Yamazaki, M.; Oishi, K.; Takeuchi, A. *Sol. Energy Mater. Sol. Cells* **2009**, *93*, 996–999.
(19) Moriya, K.; Watabe, J.; Tanaka, K.; Uchiki, H. *Phys. Status Solidi C* **2006**, *3*, 2848–2852.
(20) Tanaka, K.; Oonuki, M.; Moritake, N.; Uchiki, H. *Sol. Energy Mater. Sol. Cells* **2009**, *93*, 583–587.
(21) Tanaka, K.; Moritake, N.; Uchiki, H. *Sol. Energy Mater. Sol. Cells* **2007**, *91*, 1199–1201.
(22) Nakayama, N.; Ito, K. *Appl. Surf. Sci.* **1996**, *92*, 171–175.
(23) Madarasz, J.; Bombicz, P.; Okuya, M.; Kaneko, S. *Solid State Ionics* **2001**, 439–446.
(24) Kamoun, N.; Bouzouita, H.; Rezig, B. *Thin Solid Films* **2007**, *515*, 5949–5952.
(25) Riha, S. C.; Parkinson, B. A.; Prieto, A. L. *J. Am. Chem. Soc.* **2009**, *131*, 12054–12055.
(26) Guo, Q.; Hillhouse, H. W.; Agrawal, R. *J. Am. Chem. Soc.* **2009**, *131*, 11672–11673.
(27) Steinhagen, C.; Panthani, M. G.; Akhavan, V.; Goodfellow, B.; Koo, B.; Korgel, B. A. *J. Am. Chem. Soc.* **2009**, *131*, 12554–12555.
(28) Krunks, M.; Mikli, V.; Bijakina, O.; Rebane, H.; Mere, A.; Varema, T.; Mellikov, E. *Thin Solid Films* **2000**, *361−362*, 61–64.
(29) Amenitsch, H.; Rappolt, M.; Kriechbaum, M.; Mio, H.; Laggner, P.; Bernstorff, S. *J. Synchrotron Radiat.* **1998**, *5*, 506–508.

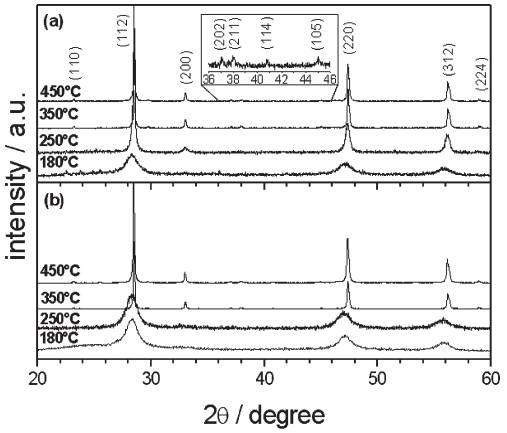

Figure 1. X-ray diffraction patterns of CZTS samples prepared with (a) 5 and (b) 3.5 equiv. of TAA at different temperatures. Diffraction patterns are shifted vertically for better visibility.

Results and Discussion

Sample Preparation. Precursor solutions were prepared from metal salts (copper(I) iodide, zinc(II) acetate, tin(II) chloride) and TAA in pyridine. To investigate the influence of the synthesizing temperature and of the amount of sulfur source on the formation of CZTS, samples with two different amounts of TAA each annealed at four different temperatures were prepared. From literature reports, it is known that an excess of thiourea is necessary to compensate the loss of sulfur during pyrolysis.[9,30] Therefore, two series of solutions containing 3.5-fold and 5-fold of a stoichiometric amount of TAA were prepared. The metal salts were applied using the stoichiometric ratio of Cu:Zn:Sn of 2:1:1. The solutions were spin-coated or sprayed onto glass substrates, which were then baked at different synthesizing temperatures between 180 and 450 °C to obtain CZTS thin films.

X-ray Diffraction. For all samples, we observed the major characteristic X-ray diffraction peaks (112), (200), (220), and (312) for the kesterite type structure of CZTS[31] (Figure 1), which shows the close relationship of the kesterite structure with the cubic sphalerite type substructure. As ZnS and Cu_2SnS_3 have a very similar crystal structure,[32] it is not possible to exclude the presence of those phases. However, the XRD patterns obtained at 350 and 450 °C also show the minor superstructure reflections of the kesterite CZTS (110), (202), (211), (114), (105), and (224) because of the high crystallinity of these powders. The positions of the reflections are in good agreement with the literature values of crystalline CZTS (kesterite), according to the Powder Diffraction File (PDF) 26−0575 of the International Centre for Diffraction Data. However, a differentiation of CZTS from Cu_2SnS_3 was only possible by the EDX analysis of the chemical composition (see below).

As Schorr et al.[33] showed by neutron diffraction studies that CZTS crystallizes in the kesterite type structure, we assume that the here prepared samples are of kesterite nature. However, it is not possible to distinguish between the Cu and Zn positions in the Cu−Zn layer in the kesterite type structure with laboratory XRD data, due to the very similar scattering factors of Cu and Zn. Therefore, the presence of stannite as possible modification, which has a structure very similar to that of kesterite,[27,34] cannot be fully ruled out.

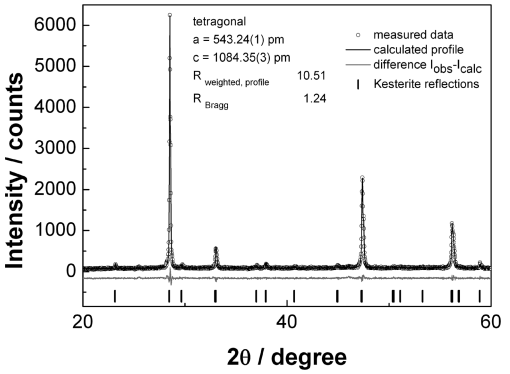

Figure 2. Results of the Rietveld refinement of the diffraction data for a sample with 5 equiv. of TAA synthesized at 350 °C; the peaks are in good agreement with the structure of kesterite CZTS (PDF 26−0575, sharp lines at the bottom).

In contrast, we were able to determine the exchange ratio of the Cu and Sn cations at their respective sites by Rietveld methods, because the scattering curves for these elements differ significantly. Generally, the calculated XRD patterns showed an excellent agreement with the measured data (Figure 2). Above 180 °C no additional peaks, corresponding to any secondary phase, can be seen, indicating that the CZTS powders are single phase. Only powders obtained at 180 °C sometimes showed some very weak unidentified reflections, which may reveal not-removed reaction side products at this temperature. This is in contrast to earlier reports, where thiourea (TU) was used as sulfur source.[6,24] In these cases, no CZTS single phase could be obtained at low temperatures.

The primary crystallite sizes of the powders rise significantly with increasing synthesizing temperature as all reflexes get sharper, which can also be seen from the domain size calculated using Scherrer formula, implemented in the TOPAS program system (Table 1). The uncertainty of these calculations is relatively high, thus it only can be a rough measure for the crystallite diameters. The data for the samples prepared at higher temperatures are in a comparable range and their differences should not be overinterpreted. However, there is a significant difference of the domain sizes at 350 and 450 °C as compared with those of the low-temperature prepared samples.

CZTS powders synthesized with only 3.5 equiv. of TAA instead of 5 equiv. of TAA show the same purity and crystal structure (kesterite). The only difference can be seen in the domain size of the samples. Powders at 180 °C can be regarded as nanocrystalline in both cases with an average size of 8 nm. However, samples containing 5 equiv. of TAA prepared at 250 °C show significantly larger

(30) Kishore Kumar, Y. B.; Suresh Babu, G.; Uday Bhaskar, P.; Sundara Raja, V. *Phys. Status Solidi A* **2009**, *206*, 1525–1530.
(31) Schaefer, W.; Nitsche, R. *Mater. Res. Bull.* **1974**, *9*, 645–654.
(32) Weber, A.; Mainz, R.; Unold, T.; Schorr, S.; Schock, H.-W. *Phys. Status Solidi C* **2009**, *6*, 1245–1248.
(33) Schorr, S.; Hoebler, H. J.; Tovar, M. *Eur. J. Mineral.* **2007**, *19*, 65–73.
(34) Paier, J.; Asahi, R.; Nagoya, A.; Kresse, G. *Phys. Rev. B: Condens. Matter Mater. Phys.* **2009**, *79*, 115126/1–115126/8.

Table 1. Lattice Parameters and Crystallographic Domain Sizes of CZTS Powders Synthesized at Different Temperatures with Different Amounts of TAA

sample	*a* (nm)	*c* (nm)	*V* (nm^3)	*d* (nm)*
		5 equiv. of TAA		
180 °C	0.5436(7)	1.095(3)	0.324(1)	8
250 °C	0.5438(1)	1.0841(4)	0.3206(2)	35
350 °C	0.54322(1)	1.08434(3)	0.31998(2)	156
450 °C	0.54335(1)	1.08496(4)	0.32032(2)	134
		3.5 equiv. of TAA		
180 °C	0.5442(5)	1.097(2)	0.3249(8)	8
250 °C	0.5438(4)	1.102(2)	0.3259(7)	9
350 °C	0.54313(2)	1.08454(5)	0.31993(2)	135
450 °C	0.54350(1)	1.08530(4)	0.32060(2)	100

*According to the Scherrer equation, refined by TOPAS.[35]

crystallites (35 nm) than the sample with 3.5 equiv. (8 nm). For higher temperatures, highly crystalline powders are obtained in both cases, with primary crystallite diameters between 100 and 160 nm.

The lattice parameters of the synthesized CZTS powders (Table 1) were obtained by the Rietveld refinements of the X-ray diffraction data. The data for the samples prepared at 350 and 450 °C, respectively, are in good agreement with the values of $a = 0.5427$ nm and $c = 1.0848$ nm, reported by Schaefer et al.[31] Samples at and below 250 °C show slightly larger lattice constants, mainly because of a cation disorder within the CZTS crystals at this temperature, leading to an expansion of the unit cell and a more or less statistically cation distribution on all possible sites.

This assumption is confirmed by the refinement of the positional parameters of the sulfur atoms, which showed that the anions are located at $x = y = 3/4$ at lower temperatures, resulting in equal metal−sulfur distances for the Cu/Zn (Cu−S, Zn−S: 233 pm) as well as for the Cu/Sn layers (Cu−S, Sn−S: 240 pm) in the structure of kesterite (Table 2). At higher temperatures, the positional parameters of the sulfur atoms differ significantly from 3/4, leading to distances of Cu1−S: 234 pm (236 pm), Sn1−S: 247 pm (244 pm), Cu2−S: 241 pm (240 pm), and Zn−S: 220 pm (222 pm) for the 350 °C samples (the distances for the 450 °C samples are given in parentheses; all standard deviations are equal or less than 1 pm). Figure 3 shows the elemental cell derived from XRD data from a sample with 5 equiv. of TAA synthesized at 350 °C. The interatomic distances do not differ significantly regarding the 3.5 and 5 equiv. of TAA samples.

In situ GIWAXS and GISAXS Analysis. The XRD results discussed above show that samples prepared at 180 °C have already a kesterite-type crystal phase. To determine at what temperature the reaction —the decomposition of thioacetamide and the formation of CZTS— starts, we performed a combined time-resolved grazing incident small and wide-angle X-ray scattering (GISAXS and GIWAXS) study on thin films in the temperature range from ambient temperature up to 180 °C.

(35) *TOPAS: General Profile and Structure Analysis Software for Powder Diffraction Data. User's Manual*; Bruker AXS, Karlsruhe, Germany, 2003.

Table 2. Positional and Site Occupancy Parameters of Kesterite CZTS (350 °C, 5 equiv. TAA); Mixed Site Occupancies For All Samples Were Refined and Are Given in the Lower Part of This Table

site	*x*	*y*	*Z*	Occupancy[a]
Cu1A	0	0	0	0.861(9)
Cu1B	1/2	1/2	1/2	0.139
Sn1A	1/2	1/2	1/2	0.861
Sn1B	0	0	0	0.139
Cu2	0	1/2	1/4	1
Zn1	1/2	0	1/4	1
S1	0.777(2)	0.744(3)[b]	0.8670(7)	1
	occ (Cu1A) = occ(Sn1A)		occ (Cu1B) = occ(Sn1B)	
		5 equiv. of TAA		
180 °C		0.7(1)		0.3
250 °C		0.6(1)		0.4
350 °C		0.861(9)		0.139
450 °C		0.84(1)		0.16
		3.5 equiv. of TAA		
180 °C		0.7(1)		0.3
250 °C		0.6(1)		0.4
350 °C		0.84(1)		0.16
450 °C		0.834(1)		0.166

[a] The occupancy parameters have been set to a sum of 1. During the refinement of the occupancies the thermal displacement parameters of the Cu1A, Cu1B, Sn1A, and Sn1B atoms have been constrained and refined with a single value. [b] The positional parameters of S1 are nearly identical in the samples heated to 350 and 450 °C, both for 3.5 equiv. of TAA and 5 equiv. of TAA. In the 180 and 250 °C samples, the refinement shifted these parameters to the ideal value of 3/4 for an disordered cubic ZnS (sphalerite) type substructure.

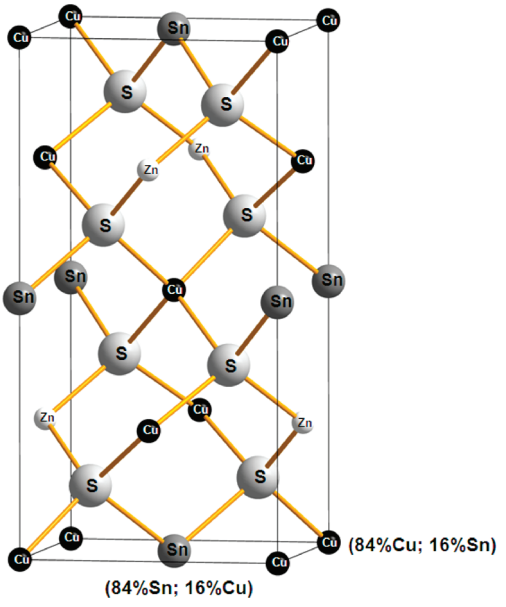

Figure 3. Elemental cell derived from XRD data from a sample with 5 equiv TAA synthesized at 350 °C. The Cu/Sn-layers show a slight cation disorder. Sixteen % of the Cu-cations are displaced by Sn-cations and vice versa.

GIWAXS patterns collected during the conversion of a precursor film containing 5 equiv TAA are shown in Figure 4. Above 105 °C, a peak at approximately 28° evolves, which corresponds to the (112) diffraction peak of CZTS kesterite structure. The slight shift of the (112) peak to smaller angles was also observed during powder-XRD measurements at lower temperatures. As already

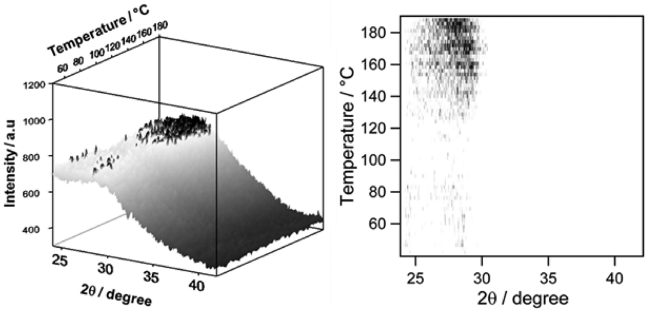

Figure 4. GIWAXS patterns of a sample containing 5 equiv. of TAA showing the (112) reflection of kesterite obtained during heating from 40 to 180 °C with a heating rate of 8 °C/min (left) and corresponding contour plot (right).

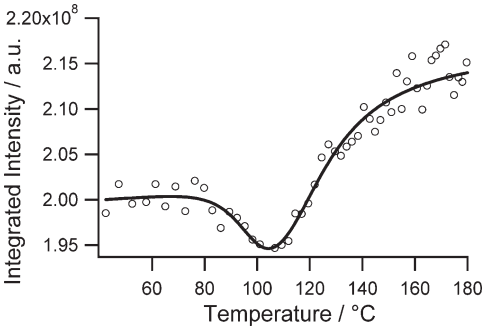

Figure 5. Lorentz corrected integrated intensity calculated from GIWAXS patterns of Figure 4 in the WAXS range between 25 and 32° 2θ, where the (112) reflection of kesterite appears. A black line is drawn as a guideline for the eye.

mentioned in the XRD discussion before, the coexistence of other similar phases like Cu_2SnS_3 or ZnS cannot be fully excluded. However, experimental results from TEM-EDX analysis and XRD analysis show a strong indication that CZTS with kesterite structure is formed, as all samples possess approximately the expected chemical composition for CZTS and powders prepared at high synthesizing temperatures (350 and 450 °C, see Figure 1) also exhibit the minor superstructure reflections for the kesterite crystal structure. Therefore, we interpret the evolving peak at approximately 28° as the (112) reflection of the kesterite structure. By plotting the Lorentz corrected integrated intensity ($\int$ dq $q^2I(q)$) from 25 to 32° 2θ versus the temperature, see Figure 5, the onset for the formation of CZTS can be estimated.

The decrease in intensity from 60 to 100 °C derives from the decomposition of TAA and TAA-complexes, whereas the sharp increase in intensity above 105 °C is assigned to the appearance of the (112) diffraction peak. On the basis of these results, the formation of CZTS from the metal and sulfur precursors starts at around 105 °C.

To probe the internal nanostructure of the films, we have taken in situ GISAXS patterns simultaneously with the GIWAXS measurements. Typical results, obtained from a sample with 5 equiv. of TAA, are shown in panels a and b in Figure 6 taken at ambient temperature and at 165 °C, respectively. Qualitatively, the evolution of the GISAXS pattern over the temperatures is visualized in Figure 6c and 6d, in which the in-plane as well as the out-of-plane scattering is presented. Both have been obtained by integration as indicated with the red boxes in Figure 6a. Here, a strong increase in the scattering intensity with temperature is visible. In particular between 80 and 120 °C the growth of the nanostructures as well as the increase of surface roughness which occurring in both directions (in-plane and out-of-plane) can be paralleled with the decomposition of TAA and TAA-complexes and the following growth of the CZTS crystallites observed in the GIWAXS data. For quantification, the out-of-plane data have been analyzed in detail, and therefore, have been fitted with a generalized unified Guinier-exponential/power-law function[36] with polymeric constrain, in which additionally a Porod term accounting for the surface roughness and large inhomogeneities was included. The whole equation writes as

$$I_{\mathrm{GISAXS}}(q_y, q_z) = G\exp\left(-\left(\frac{q^2 {R_g}^2}{3}\right)\right) + \frac{2G}{{R_g}^2}\left\{\frac{\left[\mathrm{erf}\left(\frac{qR_g}{\sqrt{6}}\right)\right]^3}{q}\right\}^P + \frac{C_{\mathrm{por}}}{q^{P_{\mathrm{por}}}}$$

in which q stands for the scattering vector calculated with $q = \sqrt{({q_y}^2 + {q_z}^2)}$. The scattering vectors in-plane and out-of-plane are denoted with q_y and q_z, correspondingly. G denotes the Guinier prefactor and R_g the radius of gyration. The parameters C_{por} and P_{por} determine the power-law contribution of the surface roughness and large inhomogeneities. In this simplified approach, the influence of refraction and correction terms of the DWBA-theory[37] have been neglected as only the structural progression was the main focus of the study.

The quality of the fit can be observed in Figure 7, in which the data are shown together with the fit. In the insert the evolution of the fit parameters with temperature is given. Interestingly there is only an increase of the radius of gyration R_g from 1.7 to 2.1 nm. This behavior has been confirmed with Laboratory SAXS experiment (see Supporting Information), in which the sample has been casted on a capillary and has been measured in transmission geometry. In this experiment the radius of gyration has been determined with 2.0 nm, which is close to the value of the GISAXS experiment taking into account different geometries and coating conditions. This demonstrates that the structural morphology of the TAA and TAA-complexes is similar to the final CTZS powder. The determined Guinier prefactor G over temperature quantifies the qualitative behavior as expected from GIWAXS and in- and out-of-plane GISAXS and manifests the increase of the electron density contrast and particle numbers caused by the CZTS formation.

(36) Beaucage, G. *J. Appl. Crystallogr.* **1995**, *28*, 717–728.

(37) Tolan, M. *X-ray Scattering from Soft Matter Thin Films*; Springer Tracts in Modern Physics; Springer-Verlag: Berlin, 1998; Vol. *148*

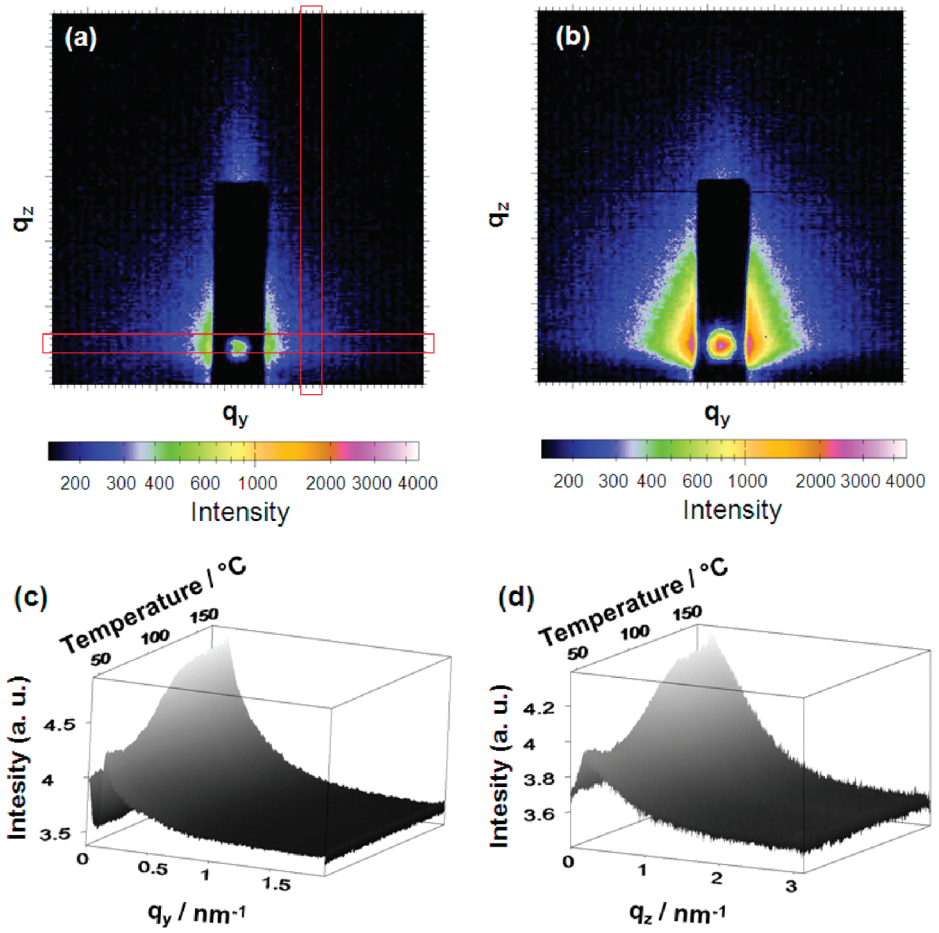

Figure 6. GISAXS patterns of the prepared samples at (a) room temperature and (b) at 165 °C. The red squares indicate the vertical and horizontal areas for integration (in-plane and out-of-plane scattering). Evolution of the in-plane scattering (c) and the out-of-plane scattering (d) as a function of temperature.

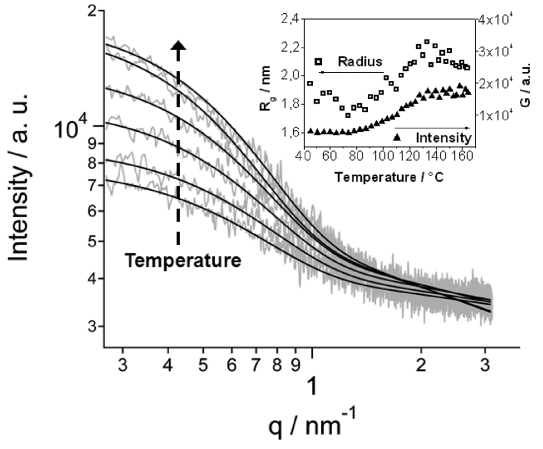

Figure 7. SAXS patterns at different temperatures (44, 83, 100, 114, 140, 164 °C) for a sample with 5 equiv. of TAA (vertical integration) and the corresponding fits. Inset shows the evolution of the Guinier prefactor G (intensity) and radius of gyration R_g during the heating run.

Assuming that the scattering structures are mainly caused by the crystalline phase, and in particular the smallest values of scattering objects are therefore the primary crystallites, the radius of gyration of 2.1 nm should be related to the crystal dimensions. Assuming spherical CZTS crystallites the diameter can be calculated using the equation $d = 2\sqrt{(5/3)}R_g$. The obtained diameter of 5.4 nm is in fairly good agreement to the diameter calculated from XRD-measurements (8 nm) taking into account that the Scherrer equation can only be seen as an estimation. In addition, GISAXS values also display a slight uncertainty because of the high surface roughness and inhomogeneity of the CZTS films and the high polydispersity of the CZTS crystallites. Summing up the GIWAXS and GISAXS results, we conclude that TAA and TAA complexes already decompose at approximately 80 °C and that the formation of CZTS starts at rather low temperatures of 105 °C.

Optical Properties. The optical properties of the synthesized CZTS films were studied by transmittance and reflectance measurements. The absorption coefficient (α) was calculated according following equation[38,39]

$$\alpha = \frac{1}{d}\ln\left(\frac{1-R}{T}\right)$$

where d is the thickness of the film, R the reflectance, and T the transmittance of the film. The film thickness was determined using a surface profiler (see Table 4).

(38) Wakkad, M. M.; Shokr, E. K.; Abd El Ghani, H. A.; Awad, M. A. *Eur. Phys. J.: Appl. Phys.* **2008**, *43*, 23–30.
(39) Khemiri, N.; Akkari, F. C.; Kanzari, M.; Rezig, B. *Phys. Status Solidi A* **2008**, *205*, 1952–1956.

Table 3. Elemental Ratios of the CZTS Powders Synthesized at Different Temperatures Calculated from TEM-EDX Measurements

	elemental ratio					
	5 equiv. TAA			3.5 equiv. TAA		
T (°C)	Cu/(Zn + Sn)	Zn/Sn	S/(Cu + Zn + Sn)	Cu/(Zn + Sn)	Zn/Sn	S/(Cu + Zn + Sn)
180	0.86 ± 0.16	1.13 ± 0.13	0.90 ± 0.07	1.00 ± 0.18	0.81 ± 0.08	0.99 ± 0.07
250	0.84 ± 0.14	1.10 ± 0.09	0.90 ± 0.06	1.04 ± 0.08	1.12 ± 0.10	0.91 ± 0.09
350	0.91 ± 0.06	1.19 ± 0.09	0.96 ± 0.07	0.92 ± 0.07	1.15 ± 0.14	0.99 ± 0.04
450	0.91 ± 0.03	1.36 ± 0.13	0.83 ± 0.04	0.89 ± 0.06	1.35 ± 0.07	0.95 ± 0.06

Table 4. R_q Values of Roughness and Thickness of the CZTS Films

	R_q values (nm)		thickness (nm)	
T (°C)	5 equiv. of TAA	3.5 equiv. of TAA	5 equiv. of TAA	3.5 equiv. of TAA
180	21.4	5.7	164	152
250	28.4	2.0	143	139
350	29.9	4.4	127	136
450	28.4	5.6	129	116

Figure 8 shows the absorption coefficient versus wavelength for the CZTS films synthesized at different temperatures with 5 and 3.5 equiv. of TAA.

All films show a high optical absorption coefficient larger than 1×10^4 cm^{-1}, which is in good agreement with other reports[6,9] in the literature. In addition, the optical band gap (E_g) values can be obtained from the following equation

$$\alpha = \frac{A(h\nu - E_g)^n}{h\nu}$$

where A is a constant, ($h\nu$) the photon energy, and n an exponent that is equal to 2 or 1/2 for indirect or direct transition, respectively. In the present work, n was found to be 1/2, indicating a direct band gap, which is consistent with the literature.[9] Therefore, the band gap values were estimated from the $(\alpha h\nu)^2$ versus ($h\nu$) plots by extrapolating the linear part of the function as shown in Figure 9.

The obtained band gaps range from 1.41 to 1.49 eV for CZTS films synthesized at 350 and 450 °C, which is consistent with reported values from the literature[7,13] (1.45 − 1.51 eV). Especially samples prepared at 180 °C exhibit a significant blue shift of the optical band gap (1.8 eV). On the one hand, this shift could be caused by quantum confinement effects as the primary crystallite size is substantially smaller at 180 °C (8 nm) than at higher temperatures (28−156 nm), as comparable critical dimensions for quantum confinement effects are reported for similar semiconductors like $CuInS_2$[40] or CdS.[41] On the other hand, it is more likely that the optical absorption is influenced by the high lattice disorder, the difference in compositional order, and/or found impurities (see Discussion below) at this temperature.

Chemical Composition. The elemental composition was determined using TEM-EDX analysis. Figure 10 shows the atomic percentage of the elements for CZTS samples synthesized with 5 and 3.5 equiv. of TAA, respectively, at different temperatures. The atom percentages were calculated using the Cu K, Zn K, Sn L, and S K peaks using the Cliff−Lorimer approximation.[42] The elemental ratios of Cu/(Zn + Sn), Zn/Sn, and S/(Cu + Zn + Sn) are summarized in Table 3.

All CZTS powders possess nearly stoichiometric amounts of sulfur, with an S/(Cu + Zn + Sn) ratio varying between 0.99 and 0.83 independent from the amount of TAA in the precursor solution. Despite the fact that the precursor solution contains stoichiometric amounts of Cu, Zn, and Sn, nearly all samples show Cu/(Zn + Sn) ratios below 1 and Zn/Sn ratios above 1. These deviations from the stoichiometric composition might be caused by a preferred generation of volatile Cu species, compared to Zn and Sn, during the thermal induced CZTS formation.

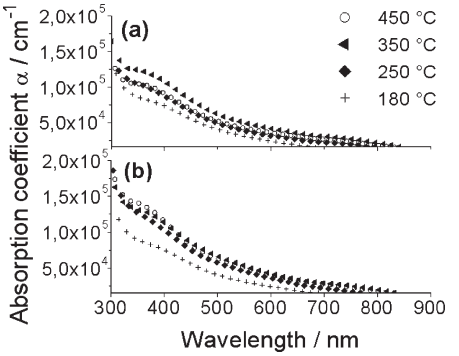

Figure 8. Optical absorption coefficient of CZTS films synthesized at different temperatures with (a) 5 and (b) 3.5 equiv. of TAA.

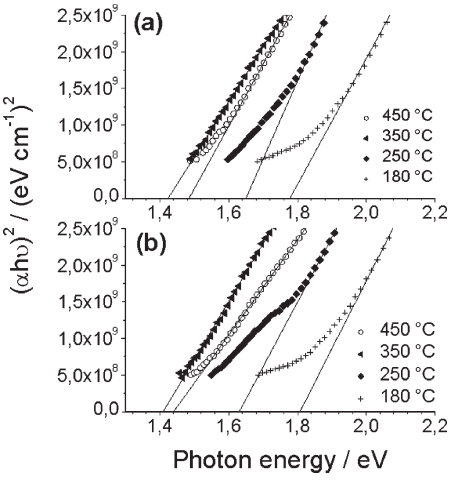

Figure 9. $(\alpha h\nu)^2$ vs photon energy ($h\nu$) of CZTS films synthesized at different temperatures with (a) 5 and (b) 3.5 equiv. of TAA.

(40) Czekelius, C.; Hilgendorff, M.; Spanhel, L.; Bedja, I.; Lerch, M.; Muller, G.; Bloeck, U.; Su, D.-S.; Giersig, M. *Adv. Mater.* **1999**, *11*, 643–646.
(41) Seoudi, R.; Shabaka, A.; Eisa, W. H.; Anies, B.; Farage, N. M. *Physica B* **2010**, *405*, 919–924.
(42) Cliff, G.; Lorimer, G. W. *J. Microsc.* **1975**, *103*, 203–207.

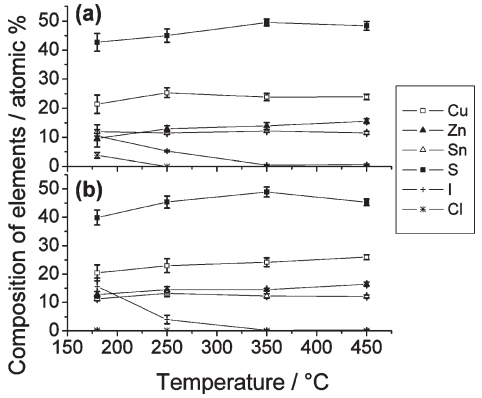

Figure 10. Chemical composition of CZTS films synthesized with (a) 5 and (b) 3.5 equiv. of TAA.

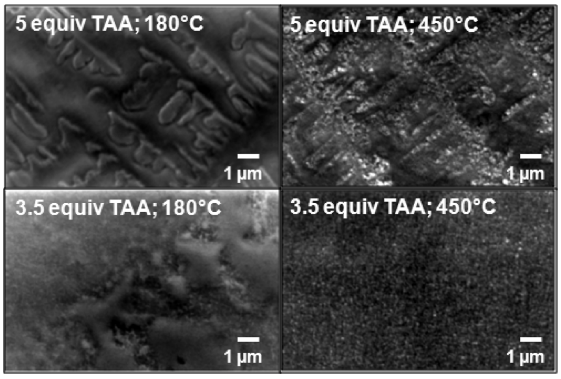

Figure 11. SEM micrographs of CZTS films synthesized with 5 and 3.5 equiv. of TAA at 180 and 450 °C.

Consequently the powders are of Cu-poor and Zn-rich nature, which is the preferable elemental composition to obtain highly efficient CZTS-based thin film solar cells according to investigations by Katagiri et al.[43] No significant influence of different synthesizing temperatures on the elemental ratios can be observed, except a slight increase in the Zn/Sn ratio when samples are heated up to 450 °C rather than 350 °C. In CZTS samples synthesized at temperatures at and below 250 °C the elements iodine and chlorine were also detected by TEM-EDX analysis, which may derive from not yet removed decomposition products of the metal precursor at these stages.

Microstructure. Figure 11 shows SEM images of the CZTS films synthesized with 5 equiv. and 3.5 equiv. of TAA, obtained at 180 and 450 °C.

Films synthesized at 180 °C show a continuous and "closed" surface, contrary to films treated with 450 °C, which exhibit a porous-like surface. CZTS films synthesized with 5 equiv TAA exhibit a microstructured surface with higher roughness in contrast to films prepared with 3.5 equiv. of TAA. Table 4 gives the root-mean-square (R_q) values of roughness based on surface profiler measurements of the films, which are consistent with the observations from the SEM micrographs showing an enhanced surface roughness for the CZTS samples prepared with 5 equiv. of TAA. The height of these structures are in the range of 20−100 nm (estimated from surface profiler measurements); however, the film itself seems to be continuous. This surface roughness and microstructure might be caused by a pronounced crystallization of excess TAA within the precursor films compared to samples with only 3.5 equiv. of TAA. This assumption is also supported by the observation that precursor films with 5 equiv. of TAA turn from transparent to white with a crystalline like surface after coating in contrast to precursor films with 3.5 equiv TAA, which stay transparent over a long time. However, only single-phase CZTS is detected by XRD-measurements in both cases at 450 °C. The film thickness decreases slightly from 164 and 152 nm to 129 and 116 nm, respectively, with increasing temperature, indicating that a more condensed CZTS layer is obtained at higher temperatures.

(43) Katagiri, H.; Jimbo, K.; Tahara, M.; Araki, H.; Oishi, K. *Mater. Res. Soc. Symp. Proc.* **2009**, 1165.

Conclusion

In this contribution, we present the preparation of highly crystalline CZTS thin films by a solution-based precursor method using copper(I) iodide, zinc(II) acetate, and tin(II) chloride as metal precursors and TAA as sulfur source, which are annealed at different temperatures. The use of TAA turns out to be advantageous as the release of sulfur species, hence the formation of sulfides already starts at 105 °C. At low synthesizing temperatures, the coexistence of other phases (ZnS, Cu_2SnS_3) besides CZTS cannot be excluded because of structural similarities; however, samples synthesized at higher temperatures (350 and 450 °C) show also the minor reflections characteristic for single-phase CZTS with kesterite structure. All films exhibit high optical absorption coefficients ($> 1 \times 10^4$ cm^{-1}) and optical band gaps between 1.41 and 1.81 eV, depending on the synthesizing temperature. Obtained CZTS powders exhibit a Cu-poor and Zn-rich nature, despite a stoichiometric precursor solution, which was found to be an ideal composition ratio for CZTS-based thin film solar cells. Samples prepared with only 3.5 equiv. of TAA exhibit a surface with low roughness, whereas the use of 5 equiv. of TAA leads to microstructured films with high surface roughness. However, both synthesis routes lead to single-phase CZTS with suitable properties for photovoltaic applications.

Acknowledgment. The authors thank the Christian Doppler Research Association (CDG) and the federal ministry of Economy, Family and Youth of Austria (BMWFJ) for financial support. GIWAXS/GISAXS experiments leading to these results have received funding from the European Community's Seventh Framework Programme (FP7/2007-2013) under grant agreement 226716. In addition, the authors thank H. Schlegl and G. Daemon for their help constructing the GIWAXS/GISAXS temperature-controlled heating cell and B. Sartori for the LabSAXS measurements.

Supporting Information Available: SAXS data (PDF). This material is available free of charge via the Internet at http://pubs.acs.org.